

IMPEDANCE STUDY AND TEM CHARACTERIZATION OF A PLD PEROVSKITE AIR ELECTRODE

Nobuyuki Imanishi, Yoshiaki Sumiya, Ken Yoshimura, Tadaaki Matsumura, Atsushi
Hirano, Yasuo Takeda, Daisuke Mori*, Ryoji Kanno*

Department of Chemistry, Faculty of Engineering, Mie University

1515 Kamihamacho, Tsu, Mie 514-8507, Japan

e-mail: imanishi@chem.mie-u.ac.jp

*Tokyo Institute of Technology

*4259 Nagatsutacho, Midoriku, Yokohama, 226-8503, Japan

Abstract

TEM observation and electron diffraction analysis of a laser ablation perovskite film was carried out. The film was deposited on a single-crystal substrate and showed epitaxial growth normal to the substrate. The crystal orientation of the perovskite film varies depending on the kind of single-crystal substrate. The surface structure of the atomic arrangement was investigated based on an analysis of electron diffraction patterns. Its relation to the kinetics of the reduction of molecular oxygen is discussed.

Keywords: SOFC, laser ablation, transmission electron microscopy, air electrode

1. Introduction

One straightforward approach to analyzing electrode processes is to simplify and idealize the cell system. A real electrode contains many components or impurities, and the active material itself has various surface morphologies, structures and defects which influence the kinetics of the reaction. A single crystal can be used to avoid these influences. In this respect, an electrode film can be epitaxially grown on a single-crystal electrolyte by the pulsed laser deposition (PLD) method. Characteristically, PLD can

form a single-crystal film on a single-crystal substrate that is crystallographically oriented in a specific direction. This kind of system produces all solid-state cells, e.g., solid oxide fuel cells(SOFCs). Recently, considerable attention has been focused on reducing the operating temperature of SOFCs, and thus there have been active studies on medium-temperature applications and kinetic studies from a fundamental perspective[1-5].

In a system in which a PLD perovskite air electrode was deposited on a single crystal of stabilized zirconia, the resistance in a series of oxygen reduction processes was discussed in a previous study [6]. This earlier study showed that PLD perovskite electrodes show the same polarization behavior as a real electrode system and exhibit a different response with the use of a different substrate. To discuss the reaction mechanism further, the structure of the PLD film must be described in greater detail. However, the film thickness is on the order of several tens of nanometers, and thus it is difficult to apply the normal X-ray diffraction (XRD) method.

In this study, the crystal structure of PLD film was analyzed by transmission electron microscopy (TEM). By combining high-resolution TEM, electron diffraction and an image-processing technique, the microstructures at specific points within the thin film can be examined. Finally, the surface structures of each ablation film and their influence on the kinetics of oxygen reduction are discussed.

2. Experimental

2.1. Sample preparation

The atomic proportions of the starting materials, La_2O_3 , SrCO_3 and Co_3O_4 , were calculated to produce $\text{La}_{0.8}\text{Sr}_{0.2}\text{CoO}_3$ (LSC) ceramic powders. Calcination of these mixtures was carried out at 1000°C for 12 h. The resultant pellets were crushed and pressed again into the desired shape using a cold isostatic press with a pressure of more than 100 bars. LSC was fired to complete the reaction using a temperature of 1300°C for

24 h. After the structure was confirmed by XRD, these sintered pellets were used as a target for laser ablation deposition.

A single crystal of Y_2O_3 -doped stabilized zirconia (YSZ) was used as the solid electrolyte of an electrochemical cell. Flat plates that measured $10 \times 10 \times 0.5 \text{ mm}$ were sliced from the ingot and polished in the crystal orientations (100), (110) and (111). These three kinds of YSZ plates were used as the substrate for LSC ablation.

The ablation of LSC was performed using a KrF excimer laser (248nm). The laser power was adjusted at 250mJ and the pulse irradiation frequency was 10Hz. The substrate temperature was kept at 700°C during the deposition. The oxygen pressure in the ablation chamber was controlled at 0.025 torr. The deposition was continued for 60 min or 8 h. The former film has a quite flat surface and was used in the electrochemical impedance analysis. The latter film was thicker and used for structural characterization by TEM.

2.2. Measurements

Platinum powder was attached to the opposite side of the LSC/YSZ plate by pasting and heating at 500°C for 2 h, and this was used as reference and counter electrodes. Thus, the following three-electrode cell was constructed:



The cell was set in an electric furnace and oxygen gas was provided at a partial pressure of 0.2atm on both sides. An electrochemical impedance analysis was then performed using a Solartron1260 frequency response analyzer and a 1287 potentiostat. An a.c. voltage of 5mV plus an open circuit potential was applied between the reference and working electrodes. The frequency was scanned decrementally from 10^6 to 0.1 Hz.

The crystal structures of the deposited LSC films were observed and analyzed by a Hitachi H-9000 TEM with a top-entry system. The accelerating voltage was 300kV. The samples were sliced normal to the plate and made thinner by the ion milling method. Cross-sections of LSC/YSZ, including their interface, could be observed. The lattice

image and selected area diffraction pattern were obtained for each sample. The above TEM system operates in high-resolution mode, and the minimum observation area has a diameter of about 1 μ m. Therefore, the observed diffraction pattern always contains diffracted spots from both YSZ and LSC. This makes it difficult to achieve an accurate index assignment of LSC. To obtain a diffraction pattern of only LSC, a pseudo pattern calculated from the real lattice image was obtained using the commercial software "Ultimage", which enables Fourier and inverse Fourier transformation between a diffraction pattern and a lattice image.

3. Results and Discussion

3.1. Impedance Analysis

Figure 1 shows Cole-Cole plots of the LSC ablation films on different single crystals. Each semicircle shows a different intercept on the real axis which indicates a different magnitude of resistance for the electrode reaction. These films are deposited on different crystal planes of YSZ, indicated by Miller indices of (100), (110) and (111). Since these films have quite flat surfaces and a thickness of only about 20nm, surface roughness can be neglected. The difference in resistance can be attributed to the different surface crystal structures of LSC film due to epitaxial growth. The order of magnitude, YSZ(100), (110), and (111), shows that the reduction of oxygen molecules occurs fastest on the LSC surface deposited on YSZ(111). This indicates that elucidation of the surface atomic structure could lead to a better understanding of the mechanism of oxygen reduction.

3.2. TEM observation of LSC/YSZ

Figure 2 shows the whole TEM image of the ablation film at low magnification. The film surface is smooth and the thickness is homogeneous. It is basically dense and free from pores. The interface between LSC and the YSZ substrate shows no empty space. The film grows continuously on the single-crystal substrate.

Since a thicker film makes the analysis easier, the 8h film was selected for the structural discussion. Figure 3 shows the cross-section of the LSC/YSZ(100) sample used in the structural analysis. The regions at the surface (a), in the middle (b), and at the interface (c) show similar lattice images. The LSC film is completely dense and has a thickness of about 80nm. The clear lattice image shows high crystallinity and continuous homogeneity for the bulk structure. The photo shows several grain boundaries running perpendicular to the substrate. The grain boundary is considered to originate as follows. First, LSC nucleation and growth occur. Island-like deposits of LSC were actually observed for short-term ablation film. Each island grows epitaxially on the substrate, while several crystal orientations are possible in the in-plane direction. When growing islands come into contact, the interface becomes a grain boundary. Under our experimental condition, a perfect single-crystal PLD film could not be obtained and they were always polycrystalline with a specific orientation. These features of the film are similar to those of other LSC films on YSZ(110) and (111) substrates.

Figure 4 (left) shows the electron diffraction pattern from the YSZ substrate. The pattern consists of strong sharp spots, since the YSZ is a single crystal. Figure 4 (right) shows the pattern of LSC/YSZ(100), which contains not only these strong spots of YSZ, but also several weak spots. These weak spots are attributed to the LSC under observation, and the intensity is related to the small volume fraction in the sample. The spot diffraction, not the ring, indicates the single-crystallinity of the LSC.

3.3. Electron diffraction analysis of YSZ

First, the crystal orientation of the YSZ substrate was discussed using the diffraction pattern in Fig. 4 (left). The calculation was based on the condition that the space group is $Fm\bar{3}m$ and the lattice parameter is $a=5.1425\text{\AA}$ for a cubic unit cell. The results are shown in Fig. 5 and Table 1. The left figure in Fig. 5 indicates spots g_1 and g_2 , which were chosen for calculation, and the distance from (000) and the angle are shown. It is possible to index g_1 and g_2 within small calculation errors, as in Table 1.

The value 0.2571nm for d_1 and d_2 is a theoretical interplanar distance obtained from a cubic unit cell with $a=5.1425\text{\AA}$. The errors next to it show the difference between the experimental data and the theoretical value. An error below 3% shows a good fit in this process, and this pattern no doubt belongs to the YSZ substrate. There are several equivalent combinations of the Miller indices for g_1 and g_2 . When [010] is taken as a zone axis and the first line in Table 1 is adopted, the arrow points to the (200) diffraction. This arrow directs the surface of the YSZ substrate in the TEM photo in Fig. 3, and (200) is parallel to the YSZ surface plane (100). This proves that the cross-section of the LSC/YSZ(100) sample was analyzed correctly. The same calculations were also carried out for LSC/YSZ(110) and LSC/YSZ(111) and the results are shown in Figs. 6 and 7 and Tables 2 and 3, respectively. These data confirm that the (110) and (111) crystal planes appear on the surface of each YSZ substrate.

3.4. Electron diffraction analysis of LSC film

To discuss the lattice orientation of the LSC film, the same calculation was carried out for the electron diffraction pattern. To distinguish the LSC diffraction spots in the pattern on the right in Fig. 4, the strong YSZ spots are connected by a broken line, as shown in Fig. 8. Other spots are diffractions that belong to LSC. They are too weak for accurate structural refinement. Therefore, in this study, a special procedure was used to discuss the crystal structure of LSC thin film. The electron diffraction pattern was directly converted from the lattice image of the LSC region by Fourier transformation using software. This mathematical pseudo diffraction pattern can be used to calculate the crystal orientation of each micro region. This calculation was carried out for all LSC/YSZ films and the following discussion concerns the case of LSC/YSZ(110). Figure 9 shows randomly selected micro regions (a) to (e) and their Fourier-transformed diffractions.

The calculated pseudo diffraction patterns are shown in Fig. 10, in which the contrast is reversed to clarify the spots. They appear to be identical to each other at all

positions. The index of each diffraction spot is calculated using pattern (e). The results are shown in Fig. 11 and Tables 4 and 5. The data sets for the space group and the lattice parameter of the sample were read from the Inorganic Crystal Structure Database (ICSD). Perovskite LSC with the R-3c space group is described in rhombohedral and hexagonal notations, which are used to calculate the theoretical values. As shown in Tables 4 and 5, both results show small fitting errors. The arrows in the middle and right figures show the surface plane of LSC growing on the YSZ(110) substrate. In the hexagonal notation, the (-300) plane grows parallel to the substrate, while in the rhombohedral system, the (-1-12) plane grows epitaxially. In the former, the other five combinations in Table 4 show the directions (-330), (030), (300), (3-30), (0-30), which are all equivalent to (-300). Similar results are seen in the rhombohedral case in Table 5. The Miller indices of these two diffractions are somewhat different, but essentially the same, as discussed below.

The diffractions of LSC/YSZ(100) and LSC/YSZ(111) were processed in the same way. In the case of LSC/YSZ(100), the surface and bulk region provide different crystal orientation. This means that epitaxial growth is not realized on YSZ(100). In contrast, LSC/YSZ(111) shows a homogeneous crystal orientation throughout the entire film. The calculation results are summarized in Table 6. They indicate that the crystal orientation of the LSC film depends on the orientation of the YSZ single crystal. A different crystal orientation of LSC leads to a different polarization behavior of the oxygen reduction process.

The hexagonal and rhombohedral notations can be mathematically transformed to each other. In this way, the hexagonal indices were converted into rhombohedral ones, which are shown in the line "H→R" in Table 6. When these values are compared to the rhombohedral indices in the next line that are directly derived from the diffraction pattern, they completely coincide, except for the surface of LSC/YSZ(100). The surface data are considered to show deviation from the bulk structure and result in an incorrect fitting calculation for the electron diffraction pattern. However, the coincidence in other

cases shows that this analysis of electron diffraction is appropriate.

3.5. Comparison with thin-film XRD results

We examined the structure of a PLD LSC film by the thin-film XRD method in the previous study, in which the out-of-plane diffraction pattern was mainly analyzed [6]. A cubic system was postulated in that analysis to calculate the crystal orientation and the lattice parameter. The thin-film XRD results show that LSCs on YSZ(100) and (111) are oriented in the LSC(110) direction, while that on YSZ(110) was not accurately determined. It is necessary to discuss the relation between the results obtained by thin-film XRD and this electron diffraction study. Therefore, index assignment under the assumption of a cubic system was carried out for the pseudo electron diffraction pattern. For the theoretical lattice parameter, the data from the thin-film XRD results were used.

Figure 12 shows the assigned indices of LSC as a cubic system in the case of LSC/YSZ(110). This shows the (-1-12) crystal plane of cubic perovskite on the surface of the film. Table 7 indicates that the fitting errors are small enough so that the index as a cubic system is possible. However, the error values are slightly larger than those in the hexagonal and rhombohedral systems. The deposited LSC is considered to be a slightly deformed cubic system. The same tendency is observed in the cases of YSZ(100) and (111) except for the surface of LSC/YSZ(100). Therefore, it is reasonable to conclude that the hexagonal system is more appropriate than a cubic system for describing the structure of LSC film, although there is only a slight difference between these two systems. The calculation results supposing a cubic system are listed together in Table 6, which show the same indices as the rhombohedral system. Thus, the orientation of LSC can be expressed in three different crystal systems, but they eventually show the same crystal plane. The calculation based on different systems leads to the same conclusion that the orientation of LSC is controlled by the orientation of the substrate.

3.6. Crystal structure model of LSC film

Structural models of LSC on three kinds of single crystal of YSZ are shown in Fig. 13. To discuss which plane appears on the surface, the illustrations are based on the results of the electron diffraction study discussed above. The structures of the crystal planes in the hexagonal, rhombohedral and cubic systems are shown. In the case of bulk LSC on YSZ(100), three indices, LSC(-210) in a hexagonal system, (-110) in a rhombohedral system and (-110) in a cubic system, are assigned. The lattice plane shown was made by slicing the crystal lattice at these calculated Miller indices. The slicing plane can be moved parallel to its normal, so the position was chosen so that the plane includes more cobalt atoms. These LSC surfaces clearly show the same arrangement of atoms.

In the case of YSZ(110), the surface plane can be LSC(-300) in the hexagonal system, (-1-12) in the rhombohedral system and (-1-12) in the cubic system. The atoms show the same arrangement. This is also confirmed in the case of YSZ(111), for which the LSC crystal planes are (-1-10), (-101) and (-101). Considering that these different indices are derived from the same material and same electron diffraction pattern, it is reasonable for these planes to show the same structure. Only LSC on YSZ(100) shows inconsistency between the hexagonal and rhombohedral structures. As discussed above, these systems did not show the same results for the index calculation.

The polarization resistance of oxygen reduction increases in the order LSC/YSZ(111), (110), (100). Its magnitude is generally influenced by the surface roughness of the electrode material. However, in this case, the ablation films used for the polarization test are prepared in a relatively short time and have a small thickness of about 20nm. Their surfaces are quite smooth and the influence of other crystal planes can be neglected. Therefore, the polarization behavior can be discussed in relation to the surface atomic arrangement. It is generally believed that oxygen molecules adsorb on cobalt ions with an empty e_g orbital. Thus, the number of cobalt and oxygen sites on the surface should be an important parameter. From the illustrations in Fig. 13, these numbers increase in the order of surface LSC/YSZ(100), LSC/YSZ(110) and LSC/YSZ(111), which coincides with

the magnitude of the polarization resistance. As a result, it is thought that the kinetics of oxygen reduction are partly determined by the planar density of cobalt and oxygen sites on the surface and this value becomes greatest in the case of YSZ(111) substrate.

4. Conclusions

An electron diffraction analysis revealed the crystal orientation of LSC ablation films. Two possible crystal systems, rhombohedral and cubic, were obtained for each diffracted pattern. Both systems can be applied with only a small fitting error, but the former shows better fitting results. The homogeneity of the crystal structure was confirmed by comparison at each point inside the film, using TEM and image-processing software. Regarding the difference in kinetics on three different LSC films, one possible parameter that could determine the rate of the reaction could be the number of cobalt and oxygen atoms on the LSC surface. In this discussion, several other slicing crystal faces are possible, so that a more controlled or simpler crystal plane is necessary to discuss the reaction mechanism further. Our results may reflect the average behavior of the LSC flat surface, which gives a rough view of the role of the surface atomic arrangement.

Acknowledgement

This work was supported in part by the Cooperation of Innovative Technology and Advance Research in Evolution Area (City Area) Project of the Ministry of Education, Culture, Sports, Science and Technology.

References

- [1] H. Uchida, S. Arisaka and M. Watanabe, *Solid State Ionics*, 135 (1-4), 347-351 (2000)
- [2] T. Kenjo and Y. Kanehira, *Solid State Ionics*, 148 (1-2), 1-14 (2002)

- [3] T. Kawada and K. Yashiro, *Electrochemistry*, 72 (5), 343-348 (2004)
- [4] T. Horita, K. Yamaji, N. Sakai, X.P. Xiong, T. Kato, H. Yokokawa and T. Kawada, *J. Power Sources*, 106 (1-2), 224-230 (2002)
- [5] T. Horita, K. Yamaji, N. Sakai, H. Yokokawa, T. Kawada and T. Kato, *Solid State Ionics*, 127 (1-2), 55-65 (2000)
- [6] N. Imanishi, T. Matsumura, Y. Sumiya, K. Yoshimura, A. Hirano, Y. Takeda, D. Mori , R. Kanno, *Solid State Ionics*, 174 (1-4), 245-252 (2004)

Table 1 Results of a diffraction analysis of the YSZ substrate in LSC/YSZ(100).

Reference data: Fm-3m Cubic a=5.1425Å

Zone Axis	g1	d1(nm)	g2	d2(nm)	$\theta(^{\circ})$
[0 1 0]	(-2 0 0)	0.2571nm (0.081%)	(0 0 -2)	0.2571nm (2.694%)	90.000°(-0.550°)
[0 1 0]	(0 0 -2)	0.2571nm (0.081%)	(2 0 0)	0.2571nm (2.694%)	90.000°(-0.550°)
[0 1 0]	(2 0 0)	0.2571nm (0.081%)	(0 0 2)	0.2571nm (2.694%)	90.000°(-0.550°)
[0 1 0]	(0 0 2)	0.2571nm (0.081%)	(-2 0 0)	0.2571nm (2.694%)	90.000°(-0.550°)

Table 2 Results of a diffraction analysis of the YSZ substrate in LSC/YSZ(110).

Reference data: Fm-3m Cubic a=5.1425Å

Zone Axis	g1	d1(nm)	g2	d2(nm)	$\theta(^{\circ})$
[1 -1 0]	(-1 -1 -1)	0.2969nm (3.946%)	(-1 -1 1)	0.2969nm (3.343%)	70.529° (0.739°)
[1 -1 0]	(1 1 1)	0.2969nm (3.946%)	(1 1 -1)	0.2969nm (3.343%)	70.529° (0.739°)

Table 3 Results of a diffraction analysis of the YSZ substrate in LSC/YSZ(111).

Reference data: Fm-3m Cubic a=5.1425Å

Zone Axis	g1	d1(nm)	g2	d2(nm)	$\theta(^{\circ})$
[1 -1 0]	(0 0 -2)	0.2969nm (1.834%)	(-1 -1 -1)	0.2969nm (-0.127%)	70.529° (0.369°)
[1 -1 0]	(0 0 2)	0.2969nm (1.834%)	(1 1 1)	0.2969nm (-0.127%)	70.529° (0.369°)

Table 4 Results of a diffraction analysis of the LSC film in LSC/YSZ(110).

Reference data: ICSD(La_{0.85}Sr_{0.15}CoO₃) R-3c Hexagonal a=5.446Å c=13.094Å

Zone Axis	g1	d1(nm)	g2	D2(nm)	$\theta(^{\circ})$
[0 0 1]	(1 1 0)	0.2723nm (-1.346%)	(2 -1 0)	0.2723nm (-0.516%)	60.000° (0.000°)
[0 0 1]	(2 -1 0)	0.2723nm (-1.346%)	(1 -2 0)	0.2723nm (-0.516%)	60.000° (0.000°)
[0 0 1]	(1 -2 0)	0.2723nm (-1.346%)	(-1 -1 0)	0.2723nm (-0.516%)	60.000° (0.000°)
[0 0 1]	(-1 -1 0)	0.2723nm (-1.346%)	(-2 1 0)	0.2723nm (-0.516%)	60.000° (0.000°)
[0 0 1]	(-2 1 0)	0.2723nm (-1.346%)	(-1 2 0)	0.2723nm (-0.516%)	60.000° (0.000°)
[0 0 1]	(-1 2 0)	0.2723nm (-1.346%)	(1 1 0)	0.2723nm (-0.516%)	60.000° (0.000°)

Table 5 Results of a diffraction analysis of the LSC film in LSC/YSZ(110).

Reference data: ICSD(La_{0.8}Sr_{0.2}CoO₃) R-3c Rhombohedral a=5.3807Å $\alpha=60.663^{\circ}$

Zone Axis	g1	d1(nm)	g2	d2(nm)	$\theta(^{\circ})$
[1 1 1]	(1 0 -1)	0.2717nm (-1.553%)	(1 -1 0)	0.2717nm (-0.725%)	60.000° (0.000°)
[1 1 1]	(1 -1 0)	0.2717nm (-1.553%)	(0 -1 1)	0.2717nm (-0.725%)	60.000° (0.000°)
[1 1 1]	(0 -1 1)	0.2717nm (-1.553%)	(-1 0 1)	0.2717nm (-0.725%)	60.000° (0.000°)
[1 1 1]	(-1 0 1)	0.2717nm (-1.553%)	(-1 1 0)	0.2717nm (-0.725%)	60.000° (0.000°)
[1 1 1]	(-1 1 0)	0.2717nm (-1.553%)	(0 1 -1)	0.2717nm (-0.725%)	60.000° (0.000°)
[1 1 1]	(0 1 -1)	0.2717nm (-1.553%)	(1 0 -1)	0.2717nm (-0.725%)	60.000° (0.000°)

Table 6 Summary of the LSC orientation indices derived from the electron diffraction patterns. They are shown in three crystal systems in addition to the mathematically derived rhombohedral notation (H→R).

YSZ substrate	100		110	111
	bulk	surface	surface & bulk	surface & bulk
Hexagonal	-210	-104	-300	-1-10
H → R	-110	255	-211	-101
Rhombohedral	-110	-1-11	-1-12	-101
Cubic	-110	---	-1-12	-101

Table 7 Results of a diffraction analysis of the LSC film in LSC/YSZ(110).

Reference data; Thin-film XRD result Pm-3m Cubic a=3.8221Å

Zone Axis	g1	d1(nm)	g2	d2(nm)	$\theta(^{\circ})$
[1 1 1]	(0 1 -1)	0.2703nm (-2.084%)	(1 0 -1)	0.2703nm (-1.260%)	60.000° (0.000°)
[1 1 1]	(1 0 -1)	0.2703nm (-2.084%)	(1 -1 0)	0.2703nm (-1.260%)	60.000° (0.000°)
[1 1 1]	(1 -1 0)	0.2703nm (-2.084%)	(0 -1 1)	0.2703nm (-1.260%)	60.000° (0.000°)
[1 1 1]	(0 -1 1)	0.2703nm (-2.084%)	(-1 0 1)	0.2703nm (-1.260%)	60.000° (0.000°)
[1 1 1]	(-1 0 1)	0.2703nm (-2.084%)	(-1 1 0)	0.2703nm (-1.260%)	60.000° (0.000°)
[1 1 1]	(-1 1 0)	0.2703nm (-2.084%)	(0 1 -1)	0.2703nm (-1.260%)	60.000° (0.000°)

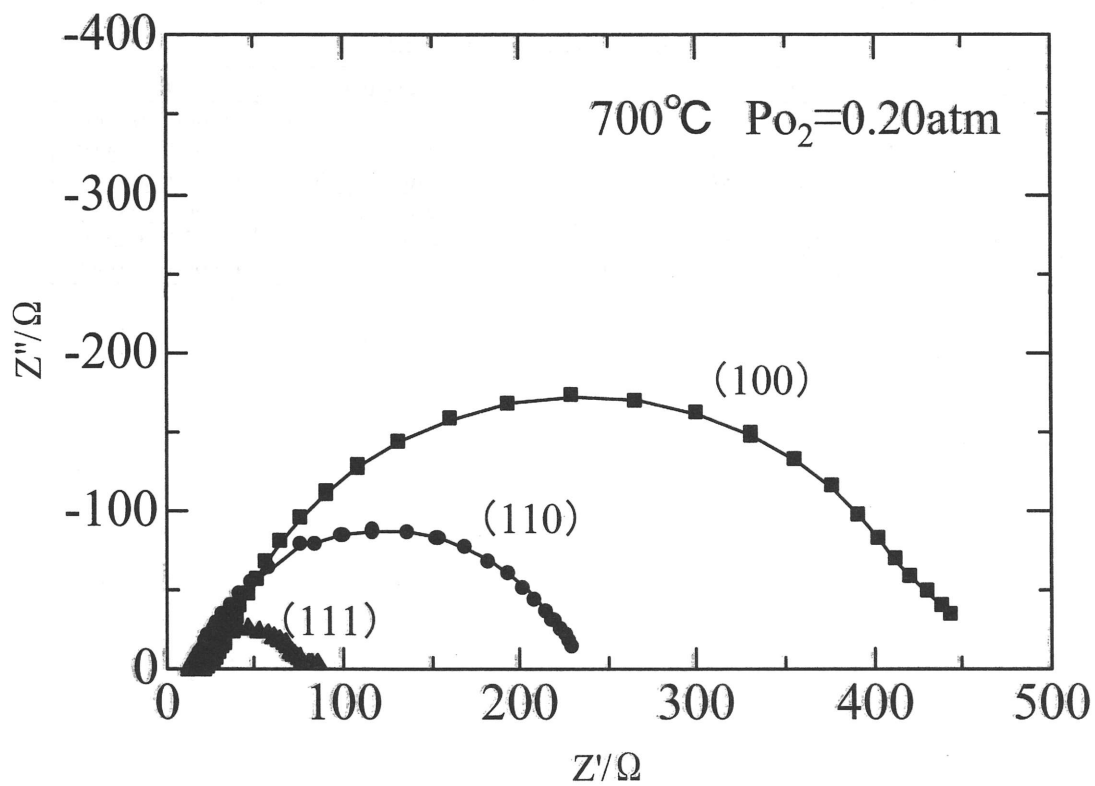


Fig. 1 Cole-Cole plots of the O_2 reduction process on an LSC ablation electrode. The three-digit number beside the spectrum shows the Miller index of the surface crystal plane of the single-crystal YSZ substrate.

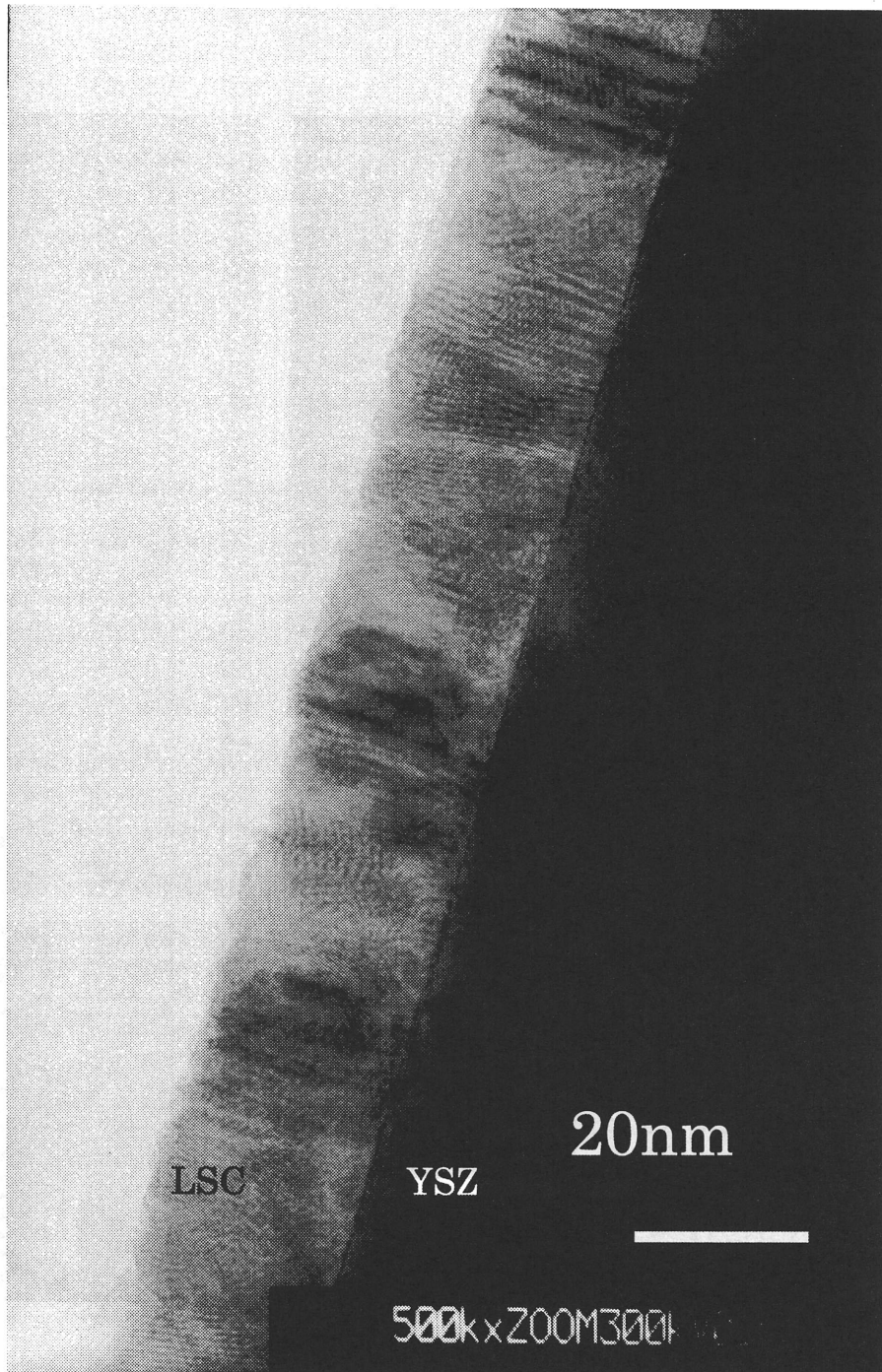


Fig. 2 TEM image of LSC/YSZ(111) ablation film.

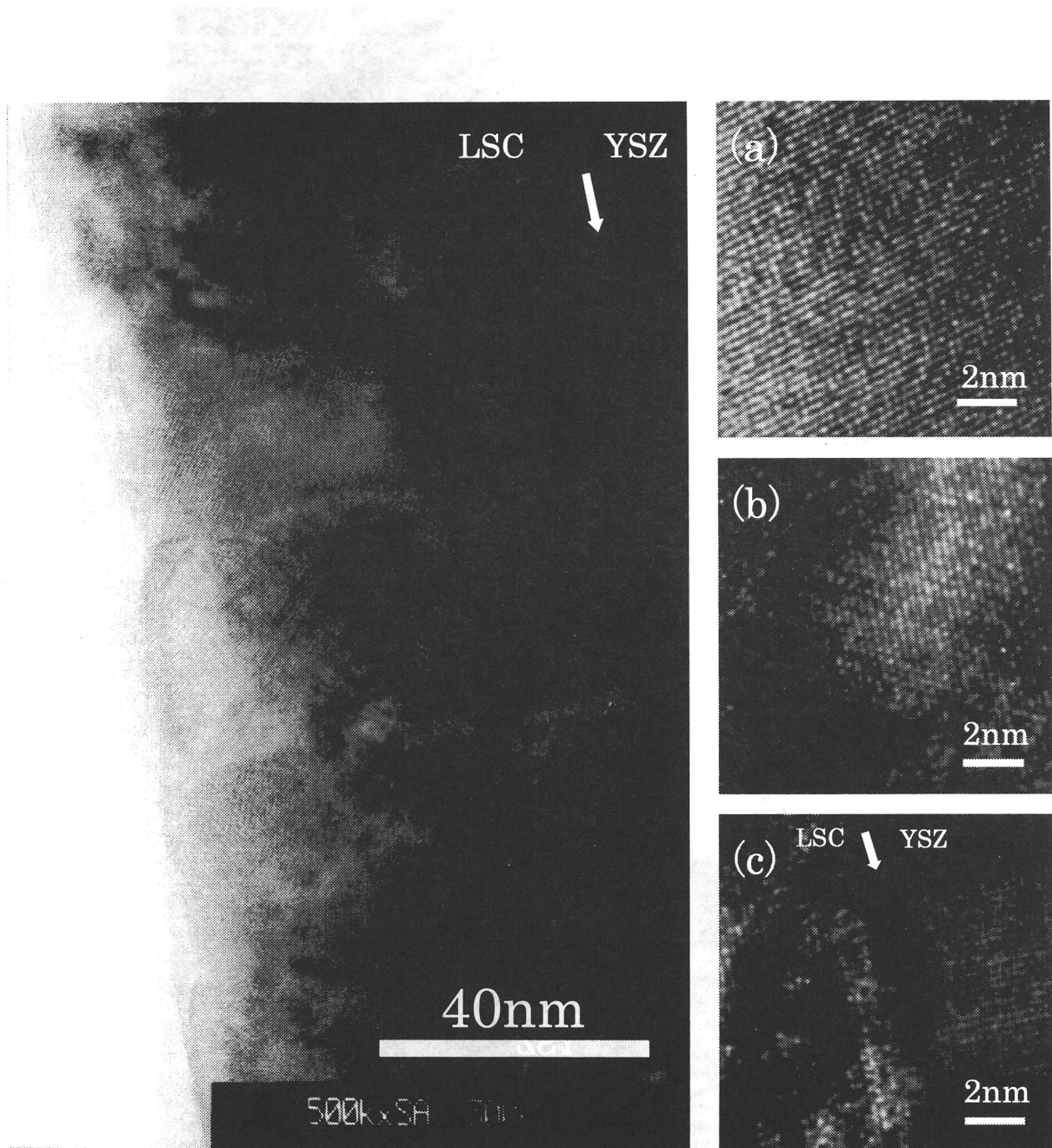


Fig. 3 TEM image of LSC/YSZ(100) ablation film. (a) enlarged photo of the surface area, (b) bulk, and (c) interface regions.



Fig. 4 Electron diffraction pattern for the YSZ substrate (left) and the pattern from the whole region including LSC/YSZ(100) (right)

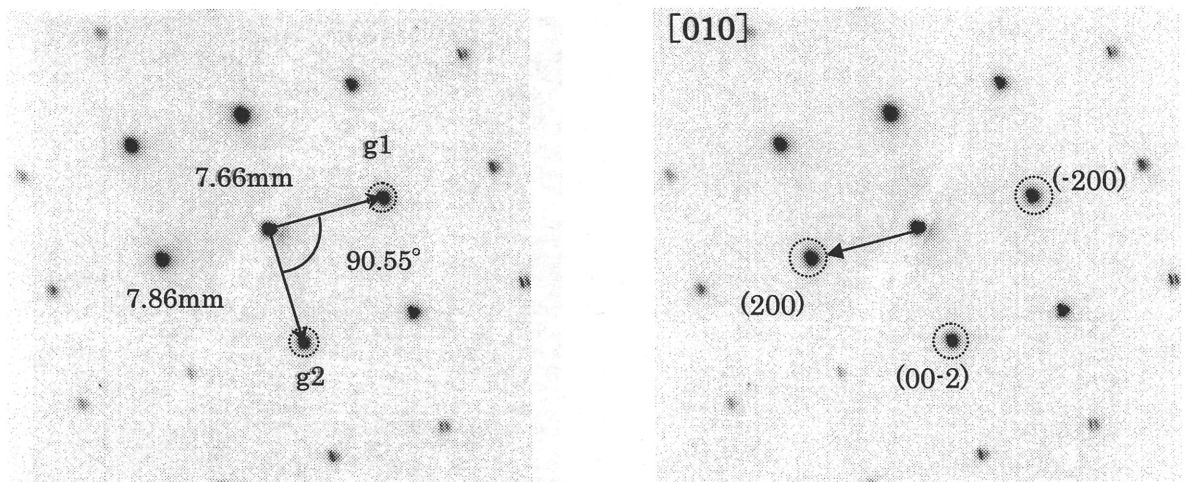


Fig. 5 Measured distance and angle of the selected points, g1 and g2, of the LSC/YSZ(100) diffraction pattern (left). The contrast is reversed for clarity. The camera distance is 1.0m. An example of the calculated indices for the same pattern (right).

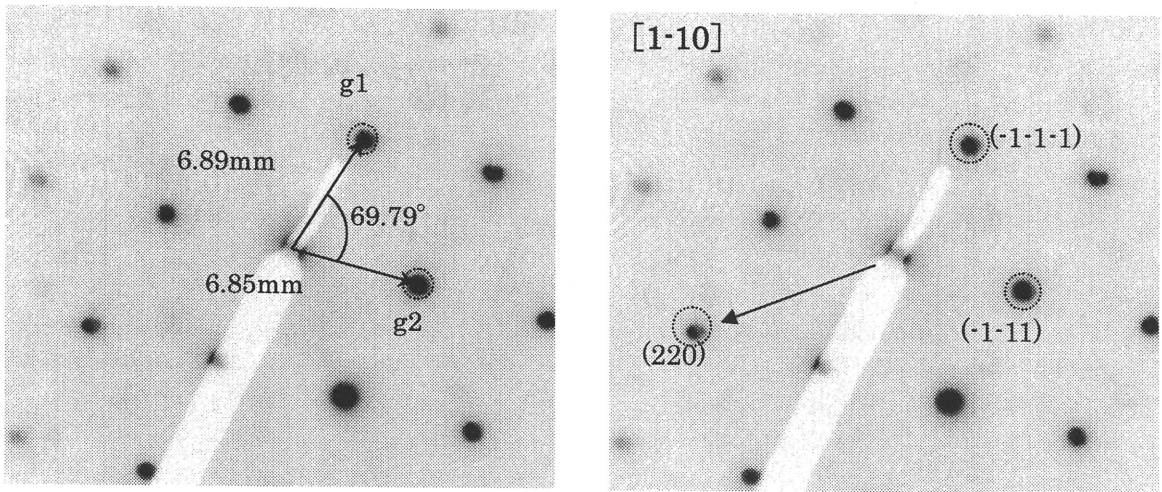


Fig. 6 Measured distance and angle of selected points, g1 and g2, of LSC/YSZ(110) diffraction pattern (left). The contrast is reversed for clarity. The camera length is 1.0m. An example of the calculated indices for the same pattern (right).

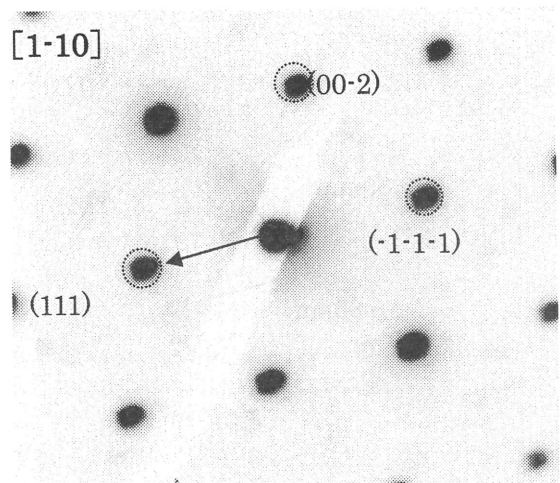
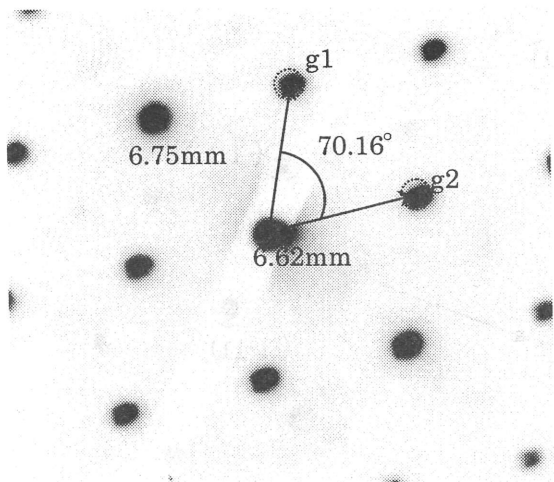


Fig. 7 Measured distance and angle of the selected points, g_1 and g_2 , of LSC/YSZ(111) diffraction pattern (left). The contrast is reversed for clarity. The camera length is 1.0m. An example of the calculated indices for the same pattern (right).

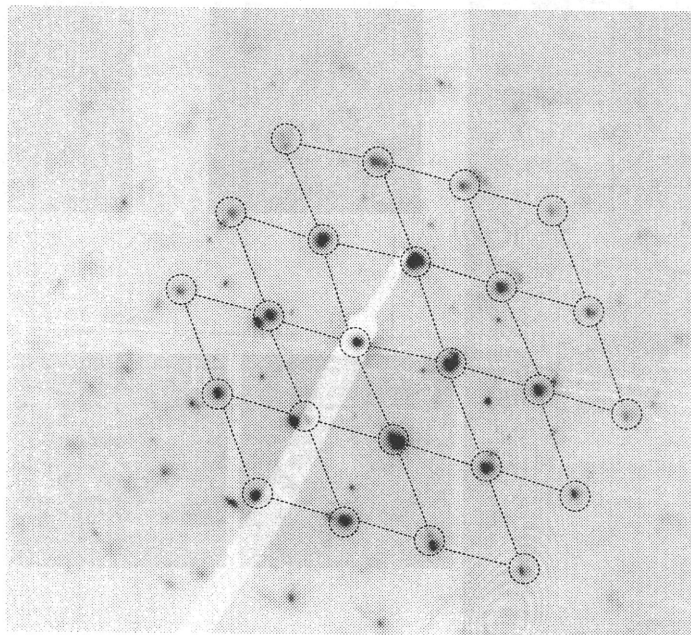


Fig. 8 Diffraction spots from YSZ in Fig. 4 (right) are connected by broken lines. Other weak spots are diffracted from the LSC film.

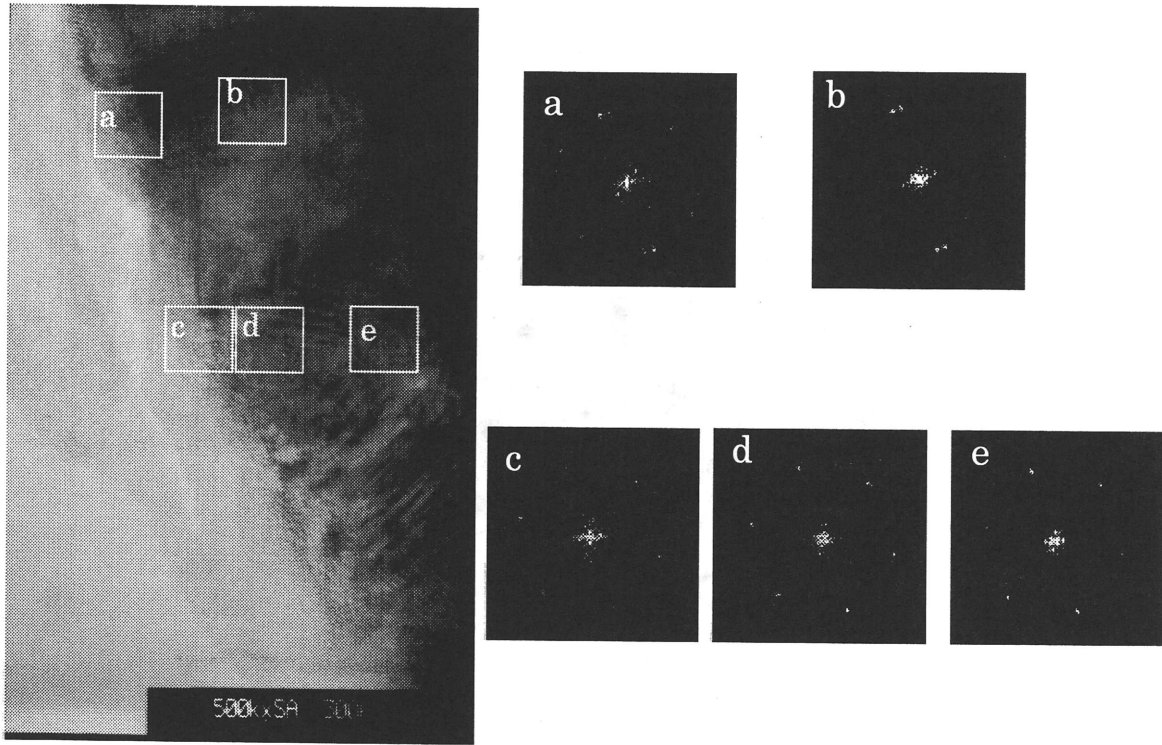


Fig. 9 Pseudo electron diffraction patterns by Fourier transform from the TEM lattice images at regions (a) to (e) of LSC/YSZ(110).

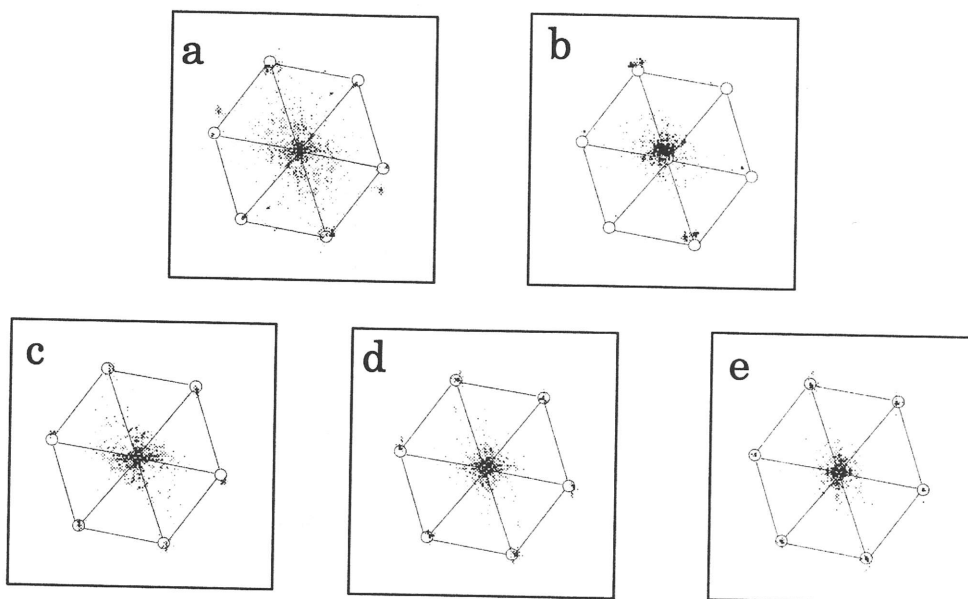


Fig. 10 Summary of the calculated pseudo diffraction patterns of regions (a) to (e). The spots are connected by broken lines.

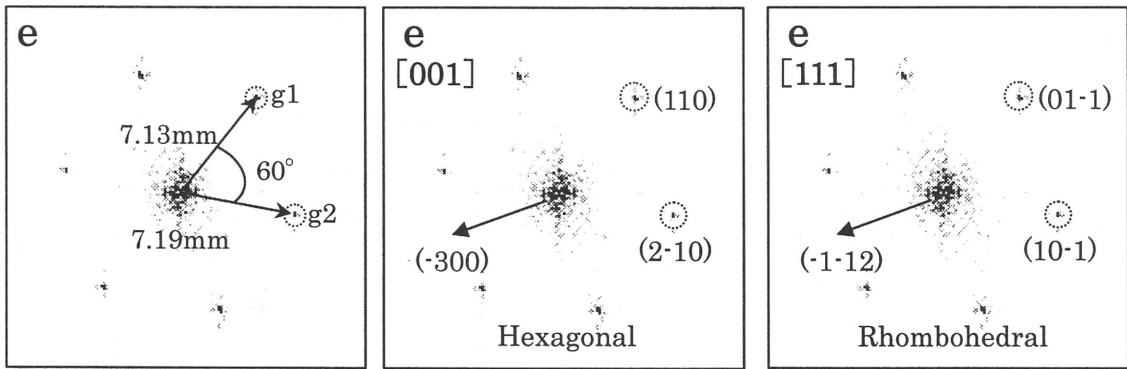


Fig. 11 Measured distance and angle of selected points, g_1 and g_2 , in the diffraction pattern of region (e) in Fig.10(left). A combination of the calculated indices in the hexagonal notation(middle) and in the rhombohedral notation(right).

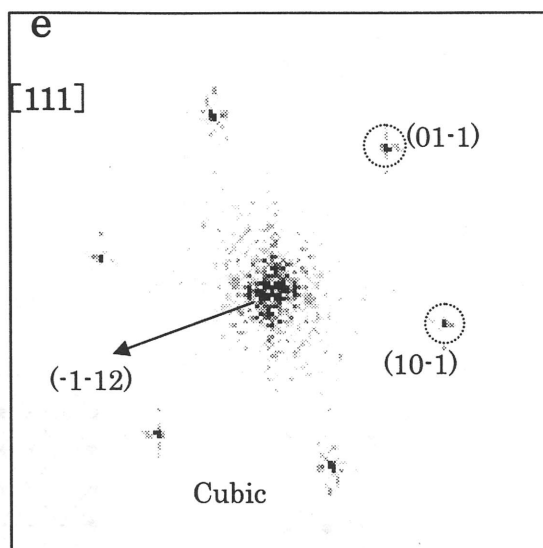


Fig. 12 The fitting result for a cubic system for the electron diffraction pattern of region (e) in Fig. 10. The geometrical data are the same as in Fig. 11 (left). The film structure is oriented in the $(-1-12)$ direction.

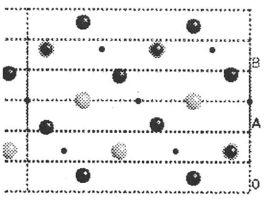
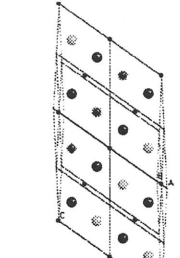
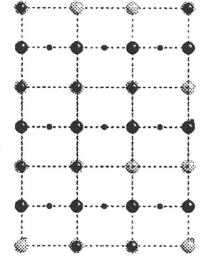
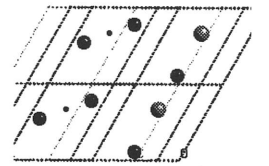
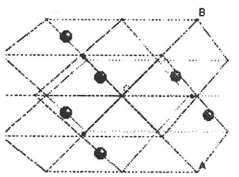
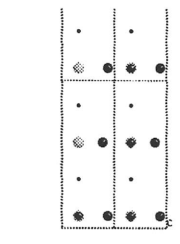
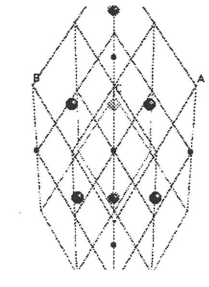
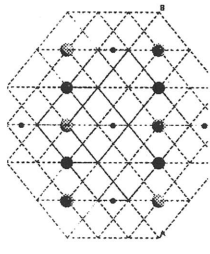
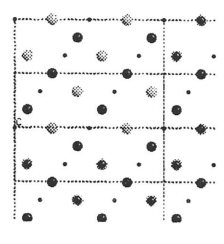
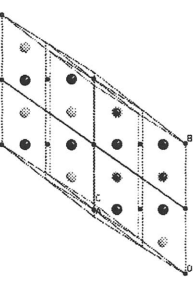
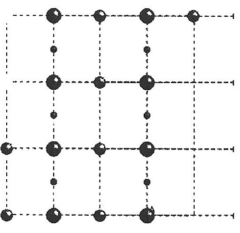
		TEM			Thin-film XRD
		Hexagonal	Rhombohedral	Cubic	Cubic
100	bulk	-210 	-110 	-110 	110
	surface	-104 	-1-11 	—	
110	surface & bulk	-300 	-1-12 	-1-12 	—
111	surface & bulk	-1-10 	-101 	-101 	110



Fig. 13 The oriented crystal structures resulting from the electron diffraction analysis. These crystal planes show one possible LSC surface. The left column shows the crystal orientation of the YSZ substrate used.